8

Heat Transfer Processes in the Rotary Kiln Bed

Thus far we have evaluated the freeboard heat transfer and quantified the radiation heat transfer to the walls and the exposed bed. The combined radiation and convection heat transfer is the total heat input into the bed. Perhaps the most important concern is what happens to the energy after it is directed to the bed. A truly complete evaluation must include the subsequent distribution of energy within the bed where the temperature dependent process that we intend to make happen takes place, at least for materials processing. We saw from the CFD modeling of pulverized fuel combustion that the temperature in the flame region, one meter around the centerline was not dramatically different from the centerline temperature (*cf*. Figure 6.15). The assumption that the freeboard is well mixed has previously been applied to rotary kilns and has allowed the use of one-dimensional modeling of the axial temperature there (Sass, 1967; Tscheng and Watkinson, 1979; and others). In fact the IFRF CEMFLAM modeling of rotary kiln flames that drew on the work of Jenkins and Moles (1981) was based on one-dimensional representation. By assuming that the bed is also well mixed and axially moves in plug flow, the axial gradients of bed temperature and gas temperature could be related to the local rates of gas-to-exposed bed and wall-to-covered bed heat transfer by ordinary differential equations (Sass, 1967). This allows one to establish a

representative "averaged" bed temperature at each axial location. One of the first early representations of one-dimensional modeling was by Sass (1967).

$$\frac{dT_s}{dz} = \frac{1}{C_{ps}G_s}\left[\alpha_2\left(T_g - T_s\right) + \alpha_3\left(T_w - T_s\right)\right] \tag{8.1}$$

$$\frac{dT_g}{dz} = \frac{1}{C_{pg}G_g}\left[\alpha_2\left(T_g - T_s\right) + \alpha_1\left(T_g - T_w\right)\right] \tag{8.2}$$

where $\alpha_i = h_i A_i$ is the product of the heat transfer coefficient h of the interface with area A, C_{pg}, and C_{ps} are the specific heats of gas and solid respectively, T is the local thermodynamic temperature, and G is the mass flow rate.

These equations formed the basis for the various one-dimensional kiln models that have appeared in the literature (Brimacombe and Watkinson, 1978; Wes et al., 1976; and others). In these models an energy balance on the wall must be included, as well as the kinetic expressions for any reactions. The latter led to a set of mass conservation expressions that must be solved along with the energy equation. For example, if the evaporation of free moisture is controlled by heat transfer, rather than mass transfer, an additional thermal balance on the moisture can be included as

$$\frac{dW}{dz} = \frac{1}{G_1\lambda}\left[\alpha_2\left(T_g - T_s\right) + \alpha_3\left(T_w - T_s\right)\right] \tag{8.3}$$

$$\lambda = \lambda_0 + C_v\left(T_g - T_s\right) \tag{8.4}$$

where W is the mass of water, λ_0 is the latent heat of liquid water, and C_v is the specific heat of water vapor.

Such models did not take into account the distribution of energy and, for that matter, temperature differences within the bed as a result of the process chemistry, bed segregation, and so on that become manifest in product quality issues. To address these one has to consider how heat is transferred to the bed, distributed, and later extracted. We saw in Chapter 7 how the heat transfer to the bed can be evaluated and how the wall takes heat from the freeboard and dumps it to the bottom of the bed (cf. Figures 7.16 and 7.17). In this chapter we will evaluate the heat transfer mechanisms between the wall and the particle bed and the redistribution of this heat and the heat from the free surface within the particle bed. These heat transfer mechanisms are the same as that

used for packed beds except that there is an effect of flow induced by the rotating wall and the flow of granules within the bed.

8.1 Heat Transfer Between the Covered Wall and the Bed

Various estimated heat transfer coefficients have been employed to calculate the covered wall-bed exchange. Evaluation of this coefficient has generally been either by pure guesswork or by adopting some type of surface renewal or penetration model. Typical guess-estimated values for the wall-solid heat transfer coefficient lie within the range of 50–100 W/m^2K (Gorog et al., 1982) which might, perhaps, depend on the kiln conditions. However, the problem at hand can be equated to that of heat transfer between a heated surface and a flowing granular material where the influence of gas within the bed might have an effect. In the absence of chemical reactions such a process might represent a kind of moving pebble-bed heat exchanger in which particles form an extended surface. One of the early models employed for the situation was based on the surface renewal-penetration theory (Wes et al., 1976) and modifications thereof (Sullivan and Sabersky, 1975). In such a case, heat conduction between a wall and granular material might be calculated using the equation for a one-dimensional unsteady state conduction

$$\frac{\partial T}{\partial t} = \alpha \frac{\partial^2 T}{\partial y^2} \tag{8.5}$$

Implicit in Equation (8.5) is that the granular material might be treated as a continuum having average or effective thermo-physical properties from which the heat transfer coefficient at the wall might be calculated as

$$h(x) = \sqrt{\frac{2nR}{x}\left(k\rho C_p\right)_{\text{eff}}} \tag{8.6}$$

where $x = 2\pi nRt$ is the distance traveled by a particle from the lower edge along the circumference of the kiln, R is the kiln radius, and n is the kiln revolution. Since these models appeared, several modifications and variations have manifested, some very complex (Barr et al., 1989; Gorog et al., 1982; Lehmberg et al., 1977). We will follow the modified penetration model for the wall-to-bed heat transfer (Figure 8.1) developed by Ferron and Singh (1991) below.

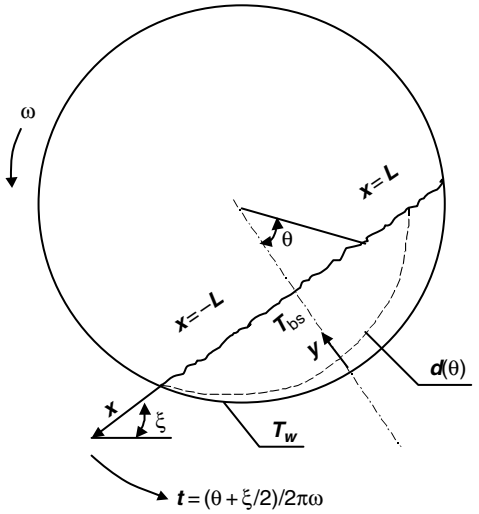

Figure 8.1 Wall-to-bed heat transfer—the modified penetration model (Ferron and Singh, 1991).

8.2 Modified Penetration Model for Rotary Kiln Wall-to-Bed Heat Transfer

Figure 8.1 presupposes that the kiln radius is large compared to the penetration depth, $d(\theta)$, that develops during contact of the heated wall coming from the exposed wall with the bed. We can set the initial conditions and boundary conditions for the solution of a two-dimensional transient heat transfer equation, similar to Equation (8.5), using the time variable in terms of the rotation as $t = (\theta + \xi/2)/2\pi\omega$, which is zero at the instant of initial wall-to-bed contact. The final time is $t = \xi/2\pi\omega$ when the wall exits the covered bed. Between the time of initial contact and the maximum time, $y = R - r$ where R is the kiln radius and r is the radius at the penetration depth, that is,

$$\text{for} \quad 0 \le t \le \xi/2\pi\omega, \quad y = R - r \tag{8.7}$$

By replacing the time variable with the subtended angle θ we can rewrite Equation (8.5) and its boundary conditions to include the degree of fill, which is in essence a function of θ.

$$2\pi\omega \frac{\partial T_b}{\partial \theta} = \alpha_b \frac{\partial^2 T_b}{\partial y^2} \tag{8.8}$$

$$T_b(0,\theta) = T_w \tag{8.9a}$$

$$T_b\left[R-\left(R^2-L^2\right)^{1/2},\theta\right] = T_{bs} \tag{8.9b}$$

$$T_b[y,\theta_0(y)] = T^-\left[-\left(y^2-2Ry+L^2\right)^{1/2},\infty\right] \tag{8.9c}$$

where $t \to \infty$ is the steady state condition, that is, when $T_b \to T_{bs}$ and

$$\theta_0(y) = -\cos^{-1}\frac{\left(R^2-L^2\right)^{1/2}}{(R-y)} \quad \text{for} \quad 0 \le y \le R-(R^2-L^2)^{1/2} \tag{8.9d}$$

The first boundary condition, Equation 8.9a, implies that we are assuming the wall and bed temperatures are equal at the initial point of contact. Also, the mean free path for the gas at the contact wall is sufficiently large that convective heat exchange by the gas is not in local equilibrium with the conduction through the bed. However, radiative heat transfer can play a vital role within the penetration layer (Ferron and Singh, 1991). As we did for the freeboard, the most practical approach is not only to solve the differential equation but to establish a heat transfer coefficient that can be used for practical calculations. The heat transfer coefficient per unit contact area may be written in terms of the overall heat balance using Newton's law of cooling,

$$h_{cw-cb} = \frac{-2LQ}{\xi R\,(T_w - T_{bs})} \tag{8.10}$$

Ferron and Singh (1991) solved the governing equations using the dimensionless temperature distribution

$$\Phi(y,\theta) = \frac{[T_b(y,\theta) - T_w]}{(T_{bs} - T_w)} \tag{8.11}$$

and found a solution to the transient equation after several mathematical manipulations as

$$\Phi(y,\theta) = erf\frac{\pi^{1/2}\zeta}{2\Delta} + 2S\sum_{j=1}^{\infty} B_j(\xi)\exp\left(-j^2\pi\zeta^2\right)\sin(j\pi\zeta) \tag{8.12}$$

for $R \gg d(\theta)$ and where

$$\zeta = \frac{y}{R-(R^2-L^2)^{1/2}} \tag{8.13a}$$

$$\Delta(\theta) = \frac{\mathrm{d}(\theta)}{R - (R^2 - L^2)^{1/2}} \tag{8.13b}$$

and

$$B_j(\xi) = \int_0^1 \sin(j\pi\zeta) \ln\left[\frac{L^*/L + \chi(\zeta)}{L^*/L - \chi(\zeta)}\right] \mathrm{d}\zeta \tag{8.14a}$$

Here, we have used a case in which the heat capacity of the bed, *mc*, is constant and the heat delivered to the free surface is independent of position, then

$$\frac{L^*}{L} = \left(1 + 8.38\frac{\omega R}{V_m}\cos\frac{\xi}{2}\right)^{1/2} \tag{8.14b}$$

where V_m is the free surface velocity.

$$\chi(\zeta) = \frac{a_2\left(\xi^2 - 2\zeta/a_2 + a_1/a_2\right)}{\sin(\xi/2)}, \tag{8.14c}$$

with $a_1 = 1 + \cos(\xi/2)$, and $a_1 = 1 - \cos(\xi/2)$.

By setting the heat balance as

$$Rk_\mathrm{b}(T_\mathrm{w} - T_\mathrm{bs}) \int_{-\xi/2}^{\xi/2} \left(\frac{\partial\Phi}{\partial y}\right)_{y=0} \mathrm{d}\theta = h_{\text{cw-cb}} R\xi (T_\mathrm{w} - T_\mathrm{bs}) \tag{8.15}$$

recognizing the Nusselt number, $Nu = h_{\text{cw-cb}} R\xi/k_\mathrm{b}$ and $Pe = R^2\xi\omega/\alpha_\mathrm{b}$

$$Nu = \frac{2\sqrt{2Pe}}{1 + \sum_{j=1}^{\infty}\left[\frac{B_j(\xi)}{\pi a_1}\right]\left[1 - \exp\left(\frac{-j^2\pi\xi^2}{2a_2^2 Pe}\right)\right]} \tag{8.16}$$

If the Peclet number is large, the sum of the denominator of Equation (8.16) does not contribute much and the heat transfer coefficient reduces to

$$Nu = 2\sqrt{2Pe} \tag{8.17}$$

Other relationships based on conventional penetration theory for packed bed have deduced that $Nu = 2^{3/2}\sqrt{Pe}$ and for low Peclet numbers to the order of 10^4, Tscheng and Watkinson (1979) deduced an empirical correlation, where $Nu = 11.6 \times Pe^{0.3}$. Any of these would suffice in estimating the wall-to-bed heat transfer coefficient as functions of the kiln's rotational speed, ω, and the dynamic angle of repose, ξ. The calculated values of Nusselt numbers using Ferron and Singh's

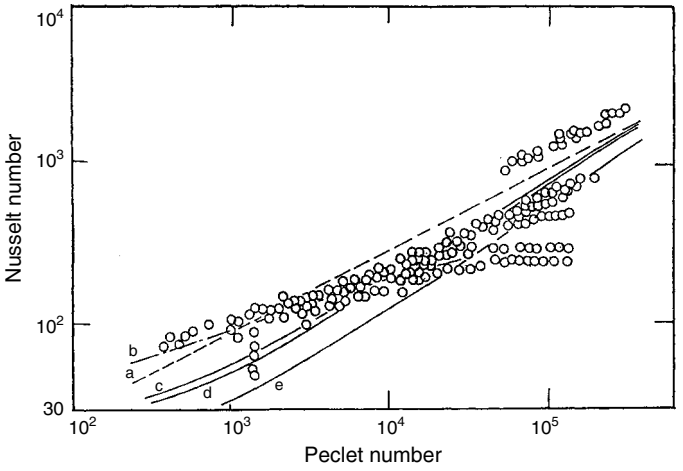

Figure 8.2 Wall-to-bed heat transfer a: $Nu = 2^{3/2}\sqrt{Pe}$; b: $Nu = 11.6 \times Pe^{0.3}$; c: $Nu = 2\sqrt{2Pe}$ at $\omega R/V_m = 0.05$ and $\xi \leq 110°$; d: $\omega R/V_m = 0.05$ and $\xi \leq 140°$; e: $\omega R/V_m = 0.05$ and $\xi \leq 180°$ (Ferron and Singh, 1991).

analytical deduction (Ferron and Singh, 1991), the classical penetration theory, and the correlation equation of Tscheng and Watkinson (1979) have been compared in Figure 8.2 (Ferron and Singh, 1991).

8.3 Effective Thermal Conductivity of Packed Beds

Heat transfer in the bed of a rotary kiln is similar to heat transfer in packed beds except that in addition to the heat flow in the particle assemblage of the static structure (Figure 8.3), there is an additional contribution of energy transfer as a result of advection of the bed material itself. The effective thermal conductivity of packed beds can be modeled in terms of thermal resistances or conductance within the particle ensemble. As shown in Figure 8.3 almost all the modes of heat transfer occurs within the ensemble, that is, particle-to-particle conduction and radiation heat transfer as well as convection through the interstitial gas depending upon the size distribution of the material and process temperature. Several models are available in the literature for estimating the effective thermal conductivity of packed beds.

We saw in Chapter 7 that the heat flow between a temperature difference ΔT across a planar gap of Δx and area A is $Q = kA\Delta T/\Delta x = UA\Delta T = G \cdot \Delta T$ where G is the conductance. If we consider the unit

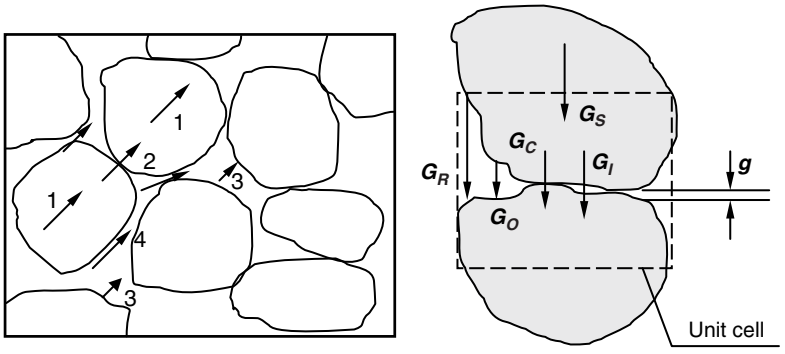

Figure 8.3 Particle ensemble for heat conductance in a static bed structure. 1. Within particle conduction. 2. Particle-particle conduction. 3. Particle-particle and gas-particle radiation. 4. Gas convection.

cell in any spherical packing as shown in Figure 8.3, it is evident that the overall conductance can be expressed as a combination of series and parallel conductances including G_S, the conductance across the solid sphere, G_C, conductance through the points of direct contact between the two spheroids, G_R, the radiation component of the heat conductance, G_I, heat flow through the inner gap of average width, g, and the conductance, G_O for the gas in the outer gap of width of the order of the radius of the spheroid. If T_1 and T_2 are the midpoint temperatures of the two spheres we can define the effective thermal conductivity over the entire cell using (Slavin et al., 2000)

$$Q = k_{\text{eff}} 4R^2 \frac{(T_1 - T_2)}{2\alpha_e R} = G(T_1 - T_2) \tag{8.18}$$

where R is the radius of the sphere and α_e is a geometrical correction factor for the conductances. Using the electrical analogy, it is evident from the flow paths in Figure 8.3 that the conductance G_S is in series with the parallel combination of G_O, G_I, and G_C, and all of which in parallel with G_R, that is,

$$G = G_R + \frac{G_S(G_O + G_I + G_C)}{G_S + (G_O + G_I + G_C)} \tag{8.19}$$

It is worth mentioning that in a vacuum, G_O and G_I are zero and since $G_S \gg G_C$, Equation (8.19) becomes $G = G_R + G_C$ (Slavin et al., 2000). The use of this equation is for all practical purposes sufficient.

The radiant heat transfer coefficient can be expressed in terms of the average temperature, $\overline{T}$ (Wakao, 1973)

$$h_{\mathrm{R}} = \frac{4\sigma\overline{T}^3}{2\left(\frac{1}{\varepsilon}-1\right)+\frac{2}{1+F_{12}}} \tag{8.20}$$

where σ is the Stefan Boltzmann constant, ε is the emissivity, and F_{12} is the view factor which was calculated as a simple cubic array by Wakao (1973) as $F_{12} = 0.151$. If the void is filled with gray gas at uniform temperature, where several gas emissivities in the void can be replaced by an average emissivity value, ε_g, then the heat transfer coefficient becomes

$$h_{\mathrm{R}}^{*} = \frac{4\sigma\overline{T}^3}{2\left(\frac{1}{\varepsilon}-1\right)+\frac{2}{1+F_{12}\left(1-\varepsilon_g\right)}} \tag{8.21}$$

For solid particles larger than 0.5 mm, that is, nonradiating gas systems, the effective thermal conductivity at atmospheric pressure is little affected by solid-solid conductivity. The Nusselt number for radiation is defined as

$$Nu = \frac{h_{\mathrm{R}} d_p}{k_{\mathrm{s}}} \tag{8.22}$$

$$k_{\mathrm{eff}} = (k_e)_{\mathrm{COND}} + (k_e)_{\mathrm{RAD}} \tag{8.23}$$

from which the effective thermal conductivity of the unit cell can be established from Figure 8.4 knowing the thermal conductivity of the solid, k_{s} and the fluid medium, k_{f}.

The radiative heat factor has been calculated using a cubic array packing with a void fraction $e = (0.5 - 0.35)$. The effective thermal conductivity involving the void fraction, which is frequently used in estimating the bed heat transfer, is expressed as (Schotte, 1960)

$$k_{\mathrm{eff}}^{r} = \frac{1-e}{\frac{1}{k_{\mathrm{s}}}+\frac{1}{4\sigma\varepsilon d_p T^3}} + e4\sigma\varepsilon d_p T^3 \tag{8.24}$$

For most applications Equation (8.24) may be adequate since the advantages of more complex models have not been extensively verified. The porosities for body-center cubic array (BCC) and face-center cubic array (FCC) are in the range of 0.3–0.25 and 0.2, respectively (Figure 8.5).

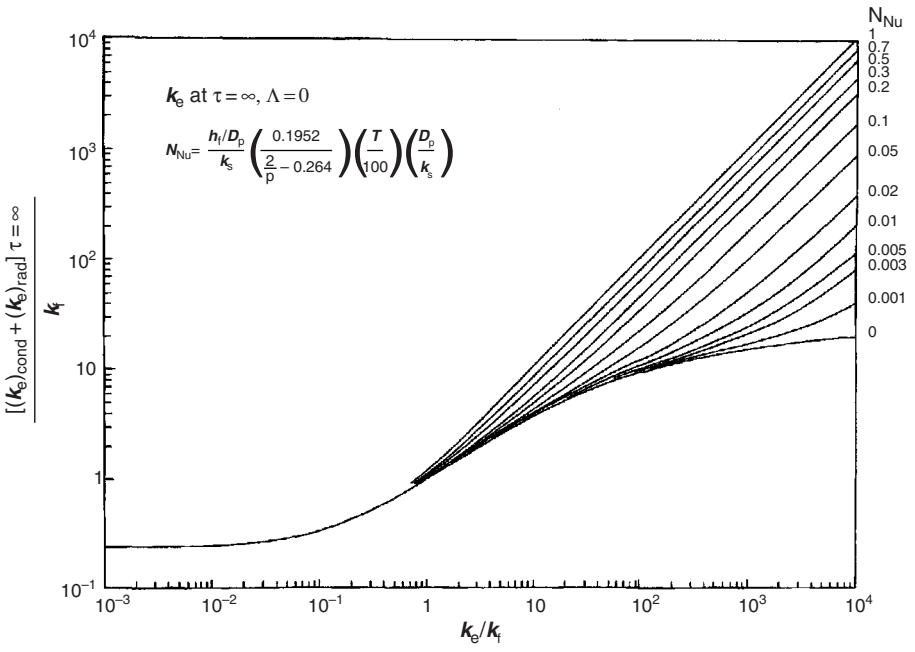

Figure 8.4 Effective thermal conductivity for packed bed medium (Wakao, 1971).

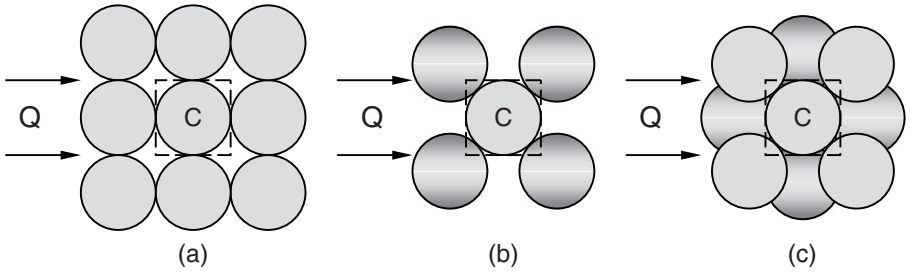

Figure 8.5 Packing arrangements for different porosity ranges. a) Simple cubic (SC), $N_C = 6 (e = 0.5 - 0.35)$. b) Body-center cubic (BCC), $N_C = 8 (e = 0.3 - 0.25)$. c) Face-center cubic (FCC), $N_C = 12 (e \leq 0.2)$.

8.4 Effective Thermal Conductivity in Rotating Bed Mode

While the effective thermal conductivity for the packed bed applies to the bulk of the bed mainly in the plug flow region, the effective conductance is enhanced by a self-diffusion coefficient component

established by the bed motion. For good mixing, this component can increase the effective heat conductance by tenfold (Boateng, 1998).

$$k'_{\text{eff}} = k_{\text{eff}} + \rho c_p \widetilde{D}_y \quad \text{or} \quad \alpha_{\text{eff}} = \alpha_e + D_y \tag{8.25}$$

where $\alpha_e = f(T_b, \nu, d_p)$, and $D_y = f(\widetilde{T}, \nu, d_p)$, and with the solid fraction $\nu = 1 - e$ and $D_y = \rho c_p \widetilde{D}_y$. $\widetilde{D}_y$ is the mass diffusion coefficient calculated in the flow model using the granular temperature. With these values, the modified effective thermal conductivity for a flowing active layer might be expressed as

$$k_{\text{eff}} = \frac{1-e}{\dfrac{1}{k_s} + \dfrac{1}{4\sigma\varepsilon d_p T^3}} + \varepsilon 4\sigma\varepsilon d_p T^3 + \frac{\rho c_p}{9\sqrt{\pi}} \frac{d_p}{(1-e)\, g_0} \widetilde{T}^{1/2} \tag{8.26}$$

It is evident from these relationships why it is preferable to feed a kiln with larger size particles as in the limestone calcination process so as to take advantage of the radiation effect enabled by the interparticle spacing. Through Equation (8.26), the effect of mixing on effective thermal conductance is achieved through two thermal diffusivities. For kiln control purposes, we can recast Equation (8.25) in the form

$$k_{\text{eff}} = \frac{k_e}{1 - Le'} \tag{8.27}$$

where $Le' = \rho c_p D_y / k_{\text{eff}}$ is a modified dimensionless Lewis number bounded by $0 \leq Le' \ll 1$. For the no flow condition, that is, as $Le' \to 0$, the effective thermal conductivity is only by packed bed. As flow is induced by rotation, superimposed on the convective transport will be particle velocity fluctuations defined by granular temperature which, like thermodynamic temperature, will enhance granular conduction through small-scale particulate mixing (Boateng, 1998).

8.5 Thermal Modeling of Rotary Kiln Processes

In Chapter 6, we considered the combustion of fuel and discussed some results of combustion modeling using CFD. In Chapter 7 we discussed heat transfer in the freeboard and the type of radiation models that go into modeling combustion and establishing freeboard temperature profiles. Having now established the physical models for

heat conduction through the bed, it is appropriate, at this time, to combine these models into a modeling process to establish the temperature and heat distribution in a rotary kiln system. Obviously, one can incorporate all these into a commercial CFD code through the help of some user-defined functions. Modeling the entire rotary kiln from the feed end to the discharge end will require the discretization of the entire freeboard space, bed, refractory walls, and so on, which not only is expensive and time-consuming but unnecessary. We saw in Chapter 6 (Figure 6.15) that the temperature profiles for the centerline and the surroundings are almost the same especially when freeboard gas mixing is optimized. This result means that we can perhaps represent the freeboard temperature distribution by a single temperature profile with little error in the calculations. It is rather the bed temperature nonuniformity that determines product quality. So we can construct a combination of one-dimensional freeboard model and use that to estimate a two-dimensional bed temperature distribution so the temperature-dependent chemical/physical reactions can be evaluated. Doing so will provide an opportunity to evaluate the effect of the flow behavior of the bed material as well as particulate mixing and segregation on the bed process. The objective of this section, therefore, is to describe the development of a thermal model for a transverse section of bed material and incorporate this two-dimensional representation of the bed into a conventional one-dimensional, plug flow type thermal model for the rotary kiln. The resultant quasi-three-dimensional thermal model is used to examine the role of the various mechanisms for heat transfer within the cross section, for example the regenerative action of the wall and the effect of the bed active layer on the redistribution of energy within the bed without resorting to CFD.

8.6 Description of the Thermal Model

A quasi-three-dimensional bed model is envisioned as one that comprises both an axial model (one-dimensional) and a cross sectional model (two-dimensional). The former is used to independently determine the one-dimensional axial temperature profiles for the freeboard gas and the bulk bed. It is implicitly assumed that the details of the energy redistribution that occurs within the bed do not significantly influence heat transfer between the bed and the freeboard. As part of the procedure for calculating these axial temperature profiles, the

surface heat flux to the bed is determined from the freeboard heat transfer and this becomes the thermal boundary condition employed to drive the cross sectional model. In doing so, the bed temperature gradient computed from the axial model is used as a sink term that represents the rate of energy removal due to the material flow in the axial direction. The one-dimensional bed temperature is also employed as a check on the mass-averaged temperature, which is estimated from the bed cross sectional model. The two-dimensional model is employed to determine the thermal condition of the bed material and the kiln wall over successive transverse sections (or slices) of the kiln and incorporates both the flow and segregation models developed in the previous chapters. The interaction of the heat transfer model with other models in the global setup for heat and mass transport calculations in the rotary kiln can be envisioned as depicted in Figure 8.6.

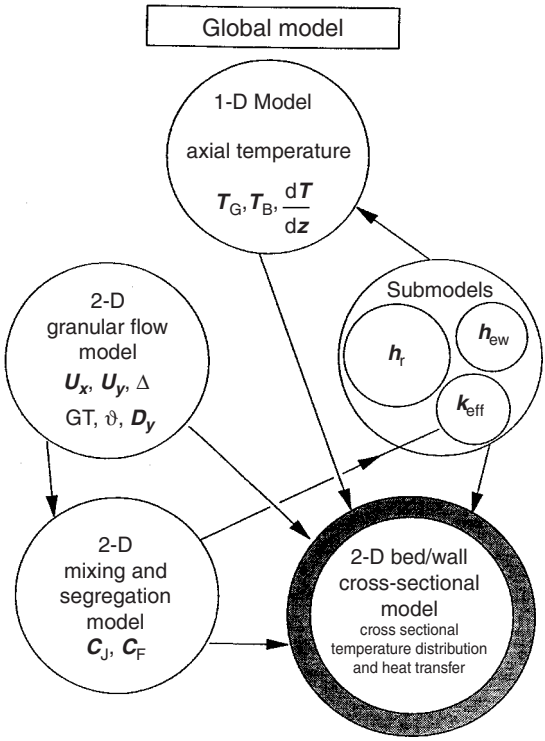

Figure 8.6 Global model layout.

8.7 One-Dimensional Thermal Model for Bed and Freeboard

Various models for the rotary kiln (Barr et al., 1989; Sass, 1967; Tscheng and Watkinson, 1978; and others) have the capability of predicting average conditions within both the bed and the freeboard as functions of axial position. The thermal component of these one-dimensional models can be derived by considering the transverse slice (Figure 8.7a), which divides the section into separate control volumes of freeboard gas and bed material. Under steady state conditions energy conservation for any control volume requires that

$$\dot{Q}_{\mathrm{NET}} = \sum (\dot{n}H)_{\mathrm{out}} - \sum (\dot{n}H)_{\mathrm{in}} \tag{8.28}$$

If conditions in the freeboard and bed are each assumed to be uniform in the transverse plane (the plug flow assumption), application

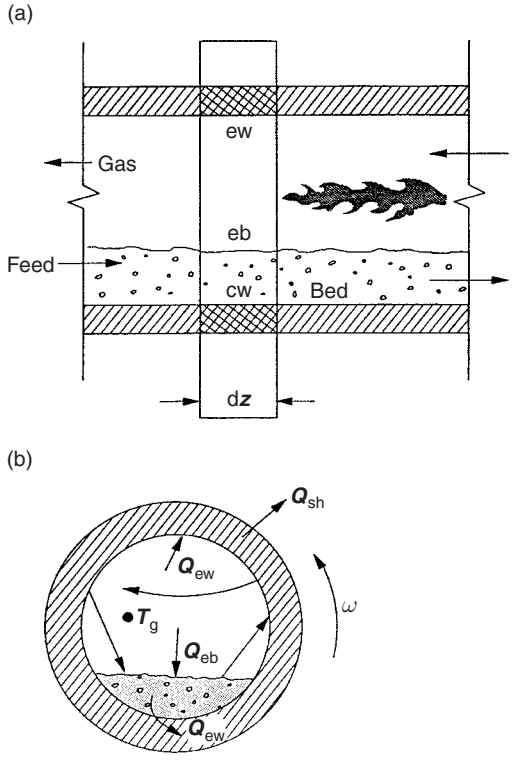

Figure 8.7 Axial and transverse slice—control volume.

of Equation (8.28) to the control volume of freeboard gas and bed material, respectively, yields a pair of ordinary differential equations relating axial gradients of temperature and composition to the net rates of heat transfer for each control volume

$$\dot{Q}_{\mathrm{g}} = \sum_{i=1}^{N_g} \left[\dot{n}_{gi} c_{p_{gi}} \frac{\mathrm{d}T_g}{\mathrm{d}z} + H_i \frac{\mathrm{d}\dot{n}_i}{\mathrm{d}z} \right] \tag{8.29a}$$

$$\dot{Q}_{\mathrm{b}} = \sum_{i=1}^{N_b} \left[\dot{n}_{bj} c_{p_{bj}} \frac{\mathrm{d}T_b}{\mathrm{d}z} + H_j \frac{\mathrm{d}\dot{n}_j}{\mathrm{d}z} \right] \tag{8.29b}$$

where N represents the total number of species in each region and T is the average or bulk temperature at that axial position.

In the absence of any chemical reaction or phase transformations these equations simplify to

$$\sum \dot{m}_{\mathrm{g}} c_{p_g} \frac{\mathrm{d}T_g}{\mathrm{d}z} = Q_{\mathrm{g}\to\mathrm{ew}} + Q_{\mathrm{g}\to\mathrm{eb}} \tag{8.30a}$$

$$\sum \dot{m}_{\mathrm{b}} c_{p_b} \frac{\mathrm{d}T_b}{\mathrm{d}z} = Q_{\mathrm{g}\to\mathrm{eb}} + Q_{\mathrm{ew}\to\mathrm{eb}} + Q_{\mathrm{cw}\to\mathrm{cb}} \tag{8.30b}$$

where the various heat transfer paths are shown in Figure 8.7b. One additional condition that must be met is that no net energy accumulation can occur within the wall. This yields an auxiliary condition

$$Q_{\mathrm{g}\to\mathrm{ew}} + Q_{\mathrm{eb}\to\mathrm{ew}} + Q_{\mathrm{cb}\to\mathrm{cw}} = Q_{\mathrm{shell}} \tag{8.30c}$$

The system of equations, Equations (8.30a,b,c), can be solved for successive axial positions by any of a variety of techniques (e.g., Runge Kutta) provided that the various heat transfer terms are characterized in terms of the local gas, bed, and wall temperatures. Thus, by starting at either end of the kiln, a complete solution of the thermal problem can be developed. It is chiefly the methodology employed in evaluating the heat transfer terms that distinguishes the various one-dimensional models.

Heat transfer at the interfacial surfaces is complex and involves radiation, convection, and at the covered bed/covered wall interface, conduction as well. Although a heat transfer coefficient can be allocated to each transport path shown in Figure 8.8 (Gorog et al., 1983) this should not obscure the difficulty associated with realistic determination of values for these coefficients. As mentioned earlier, the one-dimensional model is required only to produce a framework from which to operate

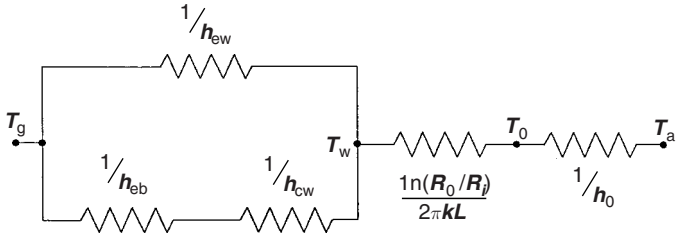

Figure 8.8 Heat transport paths and their thermal resistances.

the two-dimensional thermal model for the bed and therefore existing models can be used to evaluate heat transfer at the interfaces. In the freeboard, the radiation model in Chapter 7 is utilized to develop coefficients for radiative heat transfer, that is, $h_{r,g\rightarrow ew}$, $h_{r,g\rightarrow eb}$, $h_{r,eb\rightarrow ew}$, $h_{r,ew\rightarrow ew}$. Convection to the exposed wall and exposed bed may be calculated as per Gorog et al. (1983);

$$h_{c,ew} = 0.036\frac{k_g}{D_k}Re^{0.8}Pr^{0.33}\left(\frac{D_k}{L_k}\right)^{0.055} \tag{8.31}$$

$$h_{c,eb} = 0.4G_g^{0.62}$$

$$G_g = \frac{\dot{m}_g \times 3600}{A_g} \quad [\mathrm{kg\cdot m^2 h^{-1}}] \tag{8.32}$$

In applying these expressions the hydraulic diameter and transverse area of the freeboard must be utilized in evaluating the dimensionless groupings and mass flux terms. At the covered wall/covered bed interface the model described earlier is applied.

Since there is no intent to restrict the work to nonreactive conditions in the bed and freeboard, Equation (8.30) can be expanded to include the reactive terms, which are originally present in Equation (8.29), to yield the system

$$\left(\sum n_i c_{p_i}\right)\frac{dT_g}{dz} = h_{ew}A_{ew}\left(T_g - T_w\right) + h_{eb}A_{eb}\left(T_g - T_b\right) + \sum \gamma_i A_g \tag{8.33}$$

$$\left(\sum n_j c_{p_j}\right)\frac{dT_b}{dz} = h_{eb}A_{eb}\left(T_b - T_g\right) + h_{cw}A_{cw}\left(T_b - T_w\right) + \sum \gamma_j A_b \tag{8.34}$$

where T_b and T_w are the average temperature over the interfacial surfaces and γ are the production rates for various species involved in either chemical reactions, for example freeboard combustion or phase changes (such as evaporation of free moisture), each to be determined

by the appropriate kinetic expressions. Since mass must also be conserved for the control volumes of the bed and freeboard, a system of ordinary differential equations representing the mass balance also results from these same kinetic expressions. For example, the calcination reaction for limestone, which is

$$CaCO_3 = CaO + CO_2 \tag{8.35}$$

generates the interrelated mass balance expressions

$$\frac{d\dot{n}_{CaCO_3}}{dz} = -\frac{d\dot{n}_{CaO}}{dz} = \left(\frac{d\dot{n}_{CO_2}}{dz}\right)_{\text{freeboard}} \tag{8.36}$$

where

$$\frac{d\dot{n}_{CaCO_3}}{dz} = \gamma_{CaCO_3} A_b = A_0 \exp\left(E/\overline{R}T\right) \tag{8.37}$$

In developing the global solution for the kiln model the complete system of ordinary differential equations (i.e., the two energy balance equations, the mass balance equations, and the auxiliary energy condition for the wall) must be solved simultaneously.

8.8 Two-Dimensional Thermal Model for the Bed

Although useful results can be obtained from one-dimensional models, the assumption that conditions will be uniform across any transverse section of the bed material will hold only for a well mixed bed. Since segregation is known to occur within the bed, a two-dimensional model provides the opportunity to examine the effects of "de-mixing" within the bed on kiln performance. As we saw in Chapter 5, segregation in the transverse plane is driven by the bed motion which is established by the rotation of the kiln. However it was not until an adequate granular flow model was developed that mixing and segregation effects on temperature distribution could be modeled. For example, during rotary kiln limestone calcination, product quality is tested by checking the extent of dissociation of fine particles at the discharge end rather than larger particles. One would think that smaller particles would have a quicker thermal response and reach dissociation temperature earlier than the larger ones. However, they segregate to the core and do not see higher freeboard temperatures, due to temperature gradient across the free surface and the core.

We had mentioned earlier that the rolling bed mode would be the preferred mode of operation in most kiln processes due to its potential to achieve adequate mixing. We will set out the bed model by applying a Cartesian coordinate to the active layer since the flow there is primarily parallel to the free surface. For simplicity, we begin by first modeling an inert bed and by assuming it to behave like a continuum. Energy conservation for a control volume in the active layer (Figure 8.9a) requires that

$$\frac{\partial}{\partial x}\left(k_{\text{eff}}\frac{\partial T}{\partial x}\right)-\rho c_p u_x\frac{\partial T}{\partial x}+\frac{\partial}{\partial y}\left(k_{\text{eff}}\frac{\partial T}{\partial y}\right)-\rho c_p u_y\frac{\partial T}{\partial y}+\dot{m}_{\text{b}}c_{p_{\text{b}}}\frac{\mathrm{d}T_{\text{ba}}}{\mathrm{d}z}=0 \quad (8.38)$$

We will further assume that mixing is sufficient to ensure that, within the active layer, the temperature gradient in the axial direction of the kiln (i.e., $\mathrm{d}T_{\text{ba}}/\mathrm{d}z$) in Equation (8.38) is uniform. Since transverse mixing is at least two orders of magnitude more effective than axial mixing (Barr et al., 1989) this latter condition appears justified. The last term in Equation (8.38) includes the axial gradients of temperature in the active layer, and accounts for the removal of energy from the control volume by axial bed flow. It is assumed that all particles within the active layer advance axially at the same rate and that, because the plug flow region behaves as a rigid body, this axial advance occurs

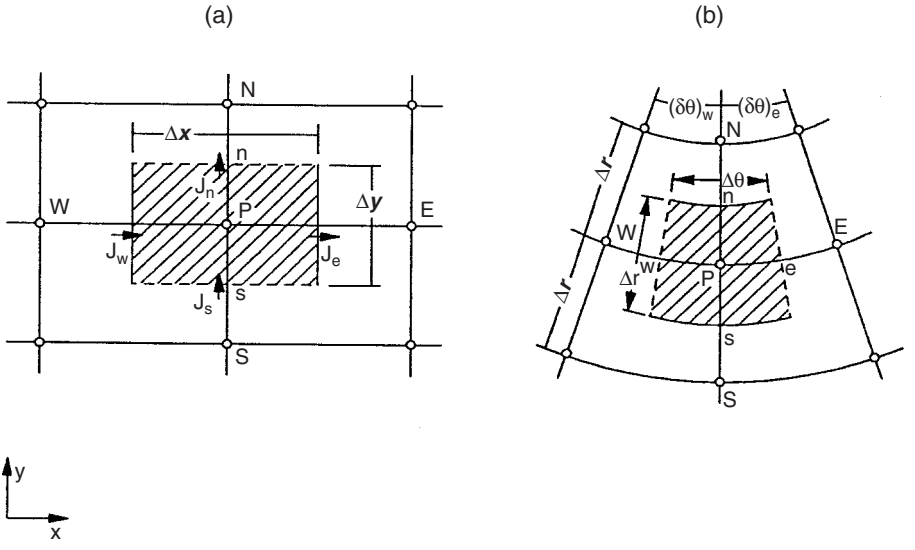

Figure 8.9 Control volumes for bed heat transfer calculations: (a) active layer; (b) plug flow region and refractory lining.

only within the active layer. Thus the mass flux $\dot{m}_b$ in Equation (8.38) is set by the kiln feed rate and the transverse area of the active layer, $\dot{m} = \dot{M}/A_{AL}$.

Because the plug flow region rotates as a rigid body about the kiln axis, a cylindrical coordinate system is employed in this region and for the refractory wall. Energy conservation for any control volume in the plug flow region and the wall (Figure 8.9b), requires that

$$\frac{\partial}{\partial r}\left(k_{pf}\frac{\partial T}{\partial r}\right)+\frac{1}{r}\frac{\partial}{\partial \theta}\left(k_{pf}\frac{\partial T}{r\partial \theta}\right)-\rho c_{p_{pf}}\omega r\frac{\partial T}{r\partial \theta}=0 \tag{8.39a}$$

$$\frac{\partial}{\partial r}\left(k_{w}\frac{\partial T}{\partial r}\right)+\frac{1}{r}\frac{\partial}{\partial \theta}\left(k_{w}\frac{\partial T}{r\partial \theta}\right)-\rho c_{p_{w}}\omega r\frac{\partial T}{r\partial \theta}=0 \tag{8.39b}$$

where the first two terms constitute the radial and transverse conduction respectively, and the third term represents the movement of energy through the control volume due to the rotation of the kiln. Since the bed particles are assumed to advance axially only in the active layer, Equation (8.39a) does not include any term for energy transport in the axial direction, it being implicitly assumed that axial conduction in the plug flow region is negligible. The effective thermal conductivity is applied with the appropriate diffusional contribution depending on the flow field.

8.9 The Combined Axial and Cross Sectional Model—The Quasi-Three-Dimensional Model for the Bed

In order to apply the understanding of the bed motion in the distribution of energy within the bed over the entire length of the kiln, we combine the two-dimensional model with a conventional one-dimensional axial model for the kiln to derive a quasi-three-dimensional model for the bed material. Although a rigorous three-dimensional formulation of the problem might be easily accomplished, the extreme aspect ratio of most kilns, $L/D \geq 10$, makes the solution of the resulting equations somewhat cumbersome. The impetus for the quasi-three-dimensional model is the need to significantly improve the capability of predicting conditions within the bed while maintaining relatively modest demands on computing capability. Two solution approaches are possible.

1. *Synchronous solution of the individual formulations*. Here, the heat transfer problem external to the bed might be determined using current values of the freeboard gas temperature and mean bed temperature. Once the net rate of heat transfer to the bed is determined (including the flux distribution to the covered wall surface) the axial gradients of the freeboard gas and mean bed temperatures become available to advance the temperatures to the next axial position by solving Equation (8.33). Before doing so the axial temperature gradient in the bed could be used to obtain a solution for Equations (8.38) and (8.39) and hence determine the temperature distribution within the bed at the current axial position.

2. *Asynchronous solution of the one-dimensional and two-dimensional problem*. The approach involves developing the one-dimensional solution over the entire kiln length before returning to the charge end to expand the axial bed temperature profile into the transverse plane. Implicit in doing so is the assumption that, at any axial position, heat transfer in the transverse plane (within the bed) will not significantly alter the freeboard, bed, and wall. The axial temperature profiles for the freeboard gas, bed, and wall are first developed using the one-dimensional model. The gas temperature and axial gradient of the bed temperature are then employed to drive the transverse model of the bed and kiln wall at a series of axial kiln positions and thereby determine, for each position, the temperature field in the bed and wall material. It should be pointed out at this stage that the two-dimensional model employs only the freeboard gas temperature and the axial bed temperature gradient at the given axial location in order to calculate the bed and wall temperatures. Both may also be supplied either from experimental data or by a one-dimensional model. Thus a check on the model can be made by comparing the computed bed and wall temperatures with either the measured values or, once the one-dimensional model has been verified, with values obtained from the latter.

8.10 Solution Procedure

The axial temperature profiles can be developed beginning from either end of the kiln by means of Equations (8.30) and (8.33). However, because direct-fired kilns operate in a countercurrent flow mode, we can employ a shooting method (Tscheng and Watkinson, 1979) to

arrive at a solution. We can start from the charge end where the material temperature is known but the gas temperature is unknown. We show an example of the calculation using an inert bed medium and a freeboard gas consisting of carbon dioxide and water vapor as the only combustion products. The thermal properties of the gas, as well as the calculation of the gray gas emissivities and absorptivities required for computing the radiation boundary conditions, are based on these two gas constituents. The exit gas temperature and composition are needed to initiate the solution (e.g., the Runge Kutta solution procedure) but the measured data may be used if available so as to avoid destabilizing the calculation as a result of the large number of unknowns involved.

At this point, the finite difference method described for convective-diffusion equations (Patanker, 1980) might be used for the solution of the governing bed/wall equations derived for the kiln cross section

$$\rho u \frac{\partial T}{\partial x_j} - \frac{\partial}{\partial x}\left(\Gamma \frac{\partial T}{\partial x_j}\right) = S \tag{8.40}$$

where S is the source term and Γ is the effective mass flux which can be given as

$$\Gamma = \frac{k_{\text{eff}}}{c_p} \quad [\text{kg/m} \cdot \text{s}]$$

Equation (8.40) may be rearranged to be

$$\frac{\partial}{\partial x_j}\left(\rho u T - \Gamma \frac{\partial T}{\partial x_j}\right) = S \tag{8.41}$$

where the term in the parentheses, represented by J_i, is the sum of the convection and diffusion fluxes. By introducing the continuity equation into the above equations, the general algebraic form of the discretized differential equations for the bed and wall become

$$A_p T_{i,j} = A_E T_{i+1,j} + A_W T_{i-1,j} + A_N T_{i,j-1} + A_S T_{i,j+1} - \dot{m} c_p \frac{\mathrm{d}T_{\mathrm{b}}}{\mathrm{d}z} \tag{8.42}$$

The coefficients, A, are expressed as

$$A_E = D_e A\,|P_e| + [-F_e, 0]$$
$$A_W = D_w A\,|P_w| + [F_w, 0]$$
$$A_N = D_n A\,|P_n| + [-F_n, 0]$$

$$A_S = D_s A\,|P_s| + [F_s, 0]$$
$$A_P = A_E + A_W + A_N + A_S \tag{8.43}$$

The heat diffusion flux, D_e, the convection flux, F_e, and the associated Peclet number are

$$D_e = \frac{\Gamma \Delta y}{\delta x_c}, \quad F_e = (\rho u_x)_{i+1,j}\,\Delta y \quad \text{and} \quad P_e = \frac{F_e}{D_e}, \text{etc.}$$

Within a numerical model, the function $A|P|$ is represented by a power law scheme as (Patanker, 1980)

$$A\,(|P|) = \left[0, \left(1 - 0.1\,|P|^5\right)\right] \tag{8.44}$$

The term in the square brackets represents the greater of the two quantities. Because of the inclusion of the source term, $\dot{m}c_p \mathrm{d}T/\mathrm{d}z$ in Equation (8.42), we multiply Equation (8.43), which represents the coefficients of the discretized equation, by c_p so as to obtain the desired units, that is, $\mathrm{W/m^{-1}\,K^{-1}}$.

For the plug flow region and the refractory wall, the discretized equations are the same as for the active region of the bed except that they are in cylindrical coordinates. For the radial direction, only the conduction component is considered and the coefficient of the algebraic (discretized) equation is equal to, for example,

$$A_S = \frac{k_{\mathrm{w}}(r\,\theta)}{\Delta R}$$

with all units being consistent with that of the term, $\dot{m}c_p \mathrm{d}T/\mathrm{d}z$.

The mesh employed for the cross sectional model is shown in Figure 8.10. Rectangular grids can be used for most of the nodes except at the interface between the plug flow and the active layer where triangular nodes automatically emerge as a result of the merging of the two coordinate systems; such nodes are considered as half of the rectangular nodes in the calculation of the nodal areas. Higher density mesh is required for the active layer of the bed and in the active region of the refractory wall. The latter is needed to capture temperature cycling that results due to kiln rotation. Although the specific depth of the wall active region is not known a priori, 10 percent is a good guess based on measurements. This value is only needed to establish the mesh because the actual depth is found from the results

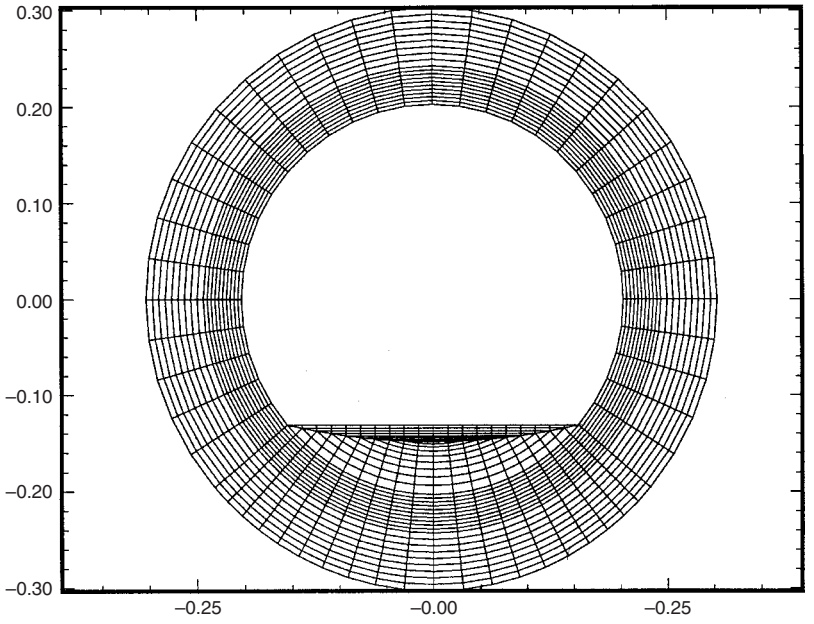

Figure 8.10 Mesh generation for cross sectional modeling.

of the numerical calculation. Outside the active wall region, a steady state one-dimensional conduction can be applied

$$Q_{SS} = 2\pi k_{\mathrm{w}} \frac{\left(T_{\mathrm{w}_r} - T_{\mathrm{w}_{r+\Delta r}}\right)}{\ln\left|(r+\Delta r)/r\right|} \tag{8.45}$$

Doing this speeds up the numerical calculation, which otherwise is slow because of the slow thermal response of the wall. From here the Gauss Siedel iteration method can be employed to solve the system of algebraic equations with a reasonable convergence criterion, for example,

$$\left|T_{ij}^{n} - T_{ij}^{n+1}\right|_{\max} < 10^{-5} \tag{8.46}$$

The solution requires an under-relaxation technique because of the numerous nonlinear temperature dependent terms. To apply the segregation of binary mixture of particles with diameter d_{pS}, with d_{pL} being the effective thermal conductivity for each node, modified by the jetsam concentration as

$$C_J(i,j)\, k_{\mathrm{eff}|_{d_{ps}}} + \left[1 - C_J(i,j)\right] k_{\mathrm{eff}|_{d_{pL}}} \tag{8.47}$$

8.11 Model Results and Application

The mathematical model presented here has been validated using a well instrumented 0.41 m diameter pilot kiln (Figure 8.11, Boateng and Barr, 1996). The predicted bed cross sectional temperature distribution for uniformly sized (well-mixed) and a binary mixture (segregated bed) in the same pilot kiln are shown in Figures 8.12 and 8.13, respectively (Boateng and Barr, 1996).

As shown, radial segregation will tend to generate a cooler region that coincides with the segregated core of fine particles. This means that, for example in limestone calcination, either the fine particles may not be fully calcined, or the larger particles at the peripheral region may be overburned at a specified freeboard gas temperature. In other processes, for example incineration of solid waste and cement clinkering, there is the possibility that the charge will contain materials of varied density. Density differences also result in segregation. These are the areas where the thermal model can be used to control the temperature nonuniformities that accompany segregation. At the moment the only means of determining bed temperature in industrial kilns is through the use of a pyrometer, which usually measures bed surface temperature only and will not detect a lower core temperature, if any segregated core exists. Therefore the kiln operator will not know whether the core materials are fully calcined until the material is discharged. The usual practice is to sample the fines in the discharge by

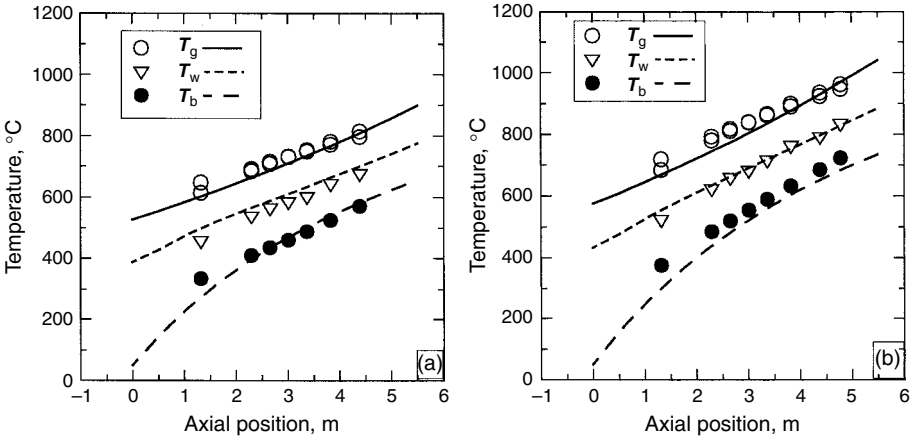

Figure 8.11 Predicted and measured temperature profiles, pilot kiln (Boateng and Barr, 1996): (a) and (b) are two different experimental measurements.

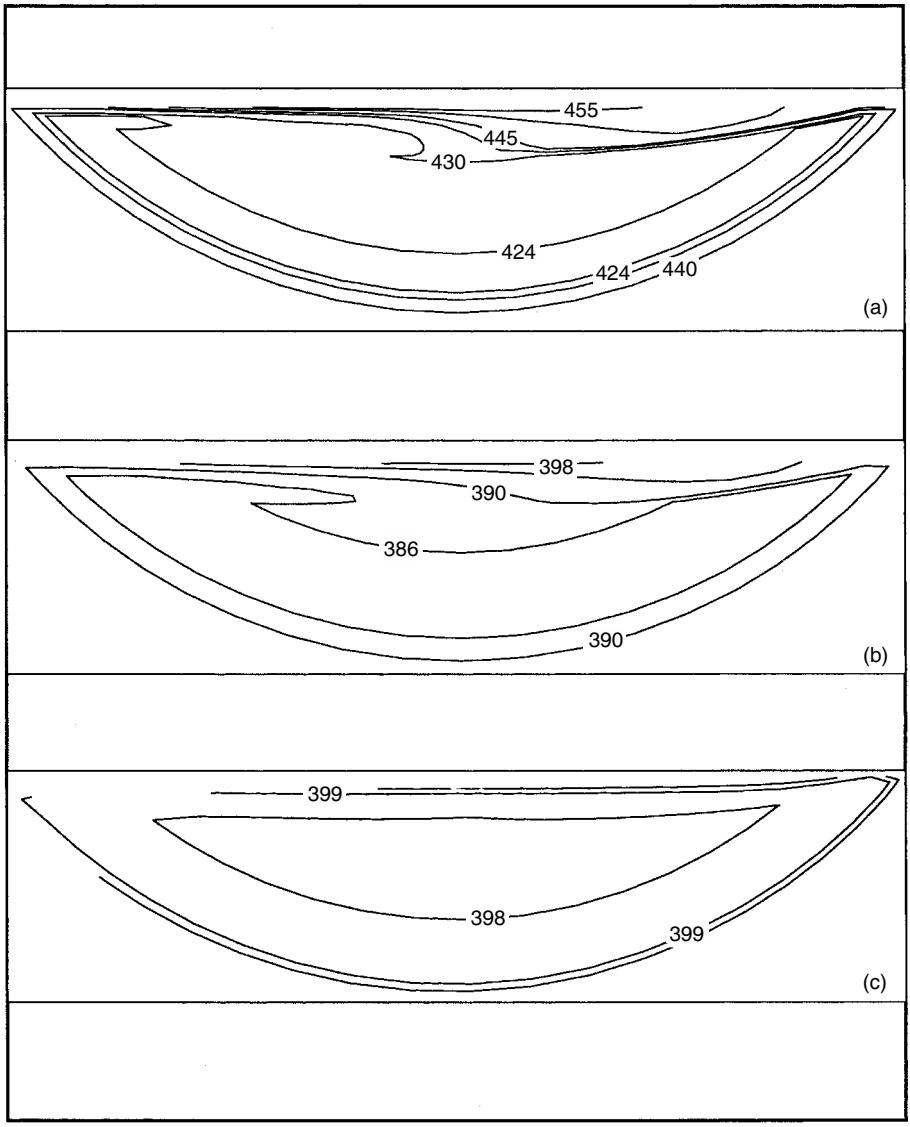

Figure 8.12 Contour plots for "mixed-bed" temperature distribution: $T_g = 631°C$, 12 percent fill: (a) 1.5 rpm, (b) 3 rpm, and (c) 5 rpm (Boateng and Barr, 1996).

breaking them apart and visually inspecting the extent of calcination or by using a dissociation test in the laboratory. A typical case follows, where the thermal model may be applied to establish the bed temperature distribution at a particular axial position and thereby evaluate the

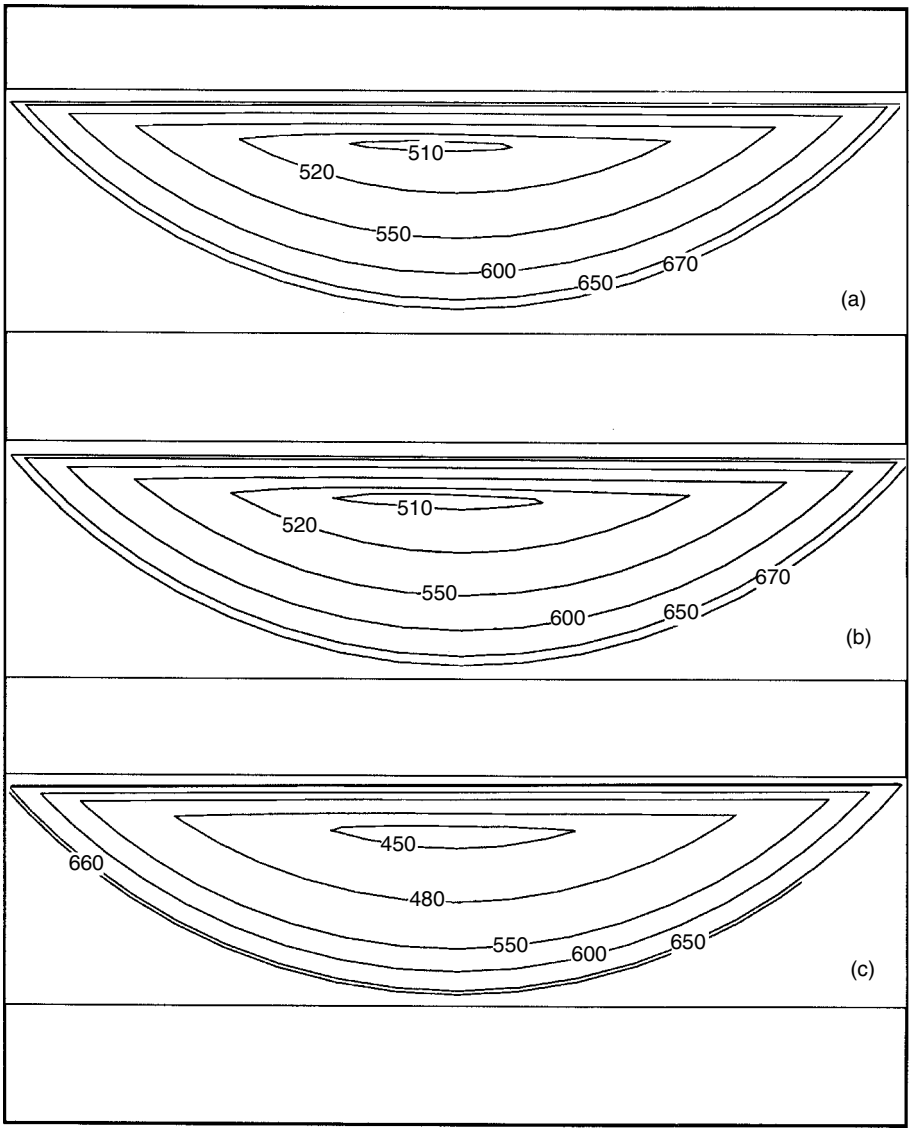

Figure 8.13 Contour plots for "segregated" temperature distribution: 12 percent fill, $T_g = 804°C$, (a) 1.5 rpm, (b) 3 rpm, and (c) 5 rpm (Boateng and Barr, 1996).

quality and energy problems that may arise as a result of segregation. If the kiln operator, upon noticing under-calcined fine particles, decides to increase the gas temperature (the obvious and usual practice), he or she will have to decide by how much the gas temperature should be

increased to. It is likely that increased gas temperature will result in an increase the of core temperature and overcook the larger particles at the periphery. In the case of density differences, for example during solid waste incineration, the particle size of the feed can be controlled by using the model to decide jetsam loading so that the material with low heat capacity will be fed as fines in order to accomplish uniform burning.

The model was applied to the process of calcining limestone in a 3 m (10 ft) diameter rotary kiln with 20 ton per hour product capacity. Figure 8.14 shows the prediction of the axial temperature and concentration profiles. Here the temperatures for the surfaces and interfaces suggest heat exchange as a function of axial location. The bed temperature strictly follows the freeboard temperature. At about 35 percent along the axial distance, the bulk bed temperature supersedes

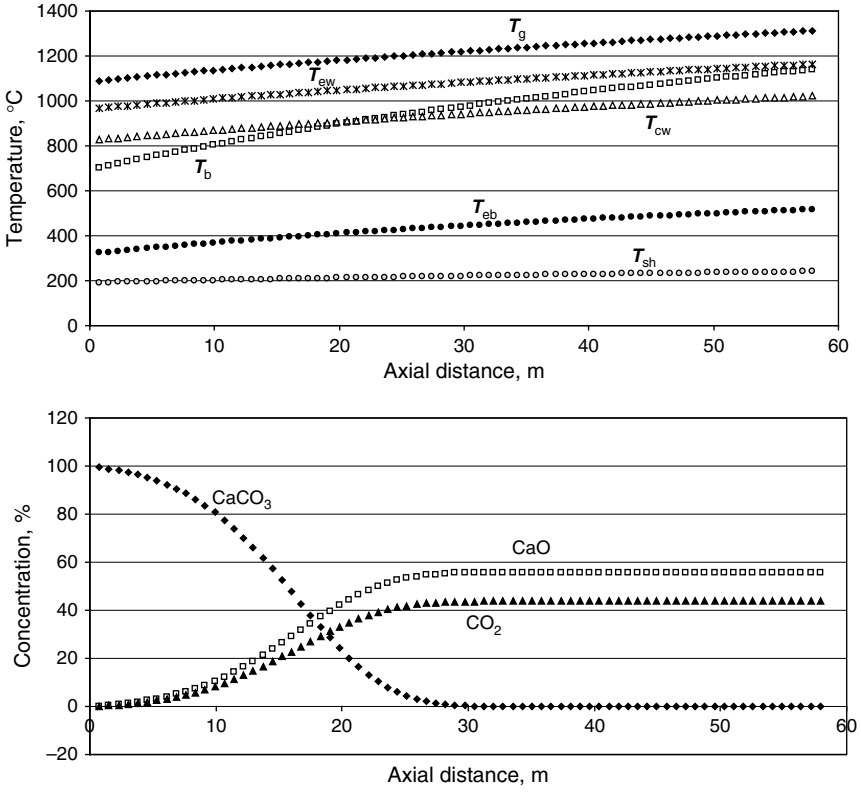

Figure 8.14 One-dimensional temperature and concentration profiles for 3.04 m (10 ft) diameter preheater kiln for limestone calcination.

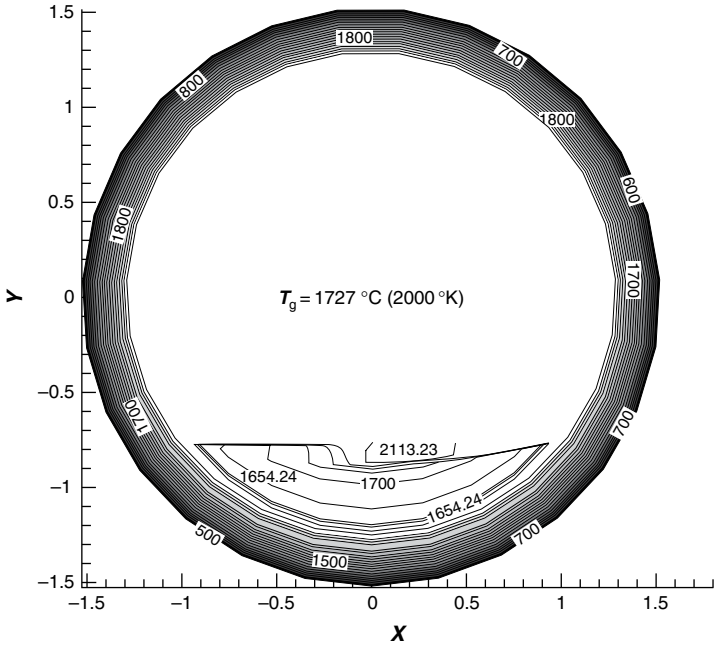

Figure 8.15 Two-dimensional temperature contours for 3.04 m (10 ft) diameter preheater kiln for limestone calcination.

the covered wall temperature showing that prior to that point the wall gives heat to the bed. The figure also shows that dissociation is complete by mid-length at least for the conditions modeled. Figure 8.15 predicts the temperature distribution in the cross section including the bed and the refractory lining at an axial location with freeboard gas temperature of 2000 K.

8.12 Single Particle Heat Transfer Modeling for Expanded Shale Processing

We had mentioned previously that most of the chemical reactions in a rotary kiln take place in the active layer. The cross sectional model shows that the extent of the reaction will depend on the exposure time. The modeling of the exposed bed heat transfer coefficients allows for the possibility of modeling the temperature response of a single particle that emerges from the plug flow region into the active layer and tumbles down the free surface. We will examine the ramification

of the time-temperature history using an expanded shale process. This process is described later in Chapter 10 but for now we will look at the material transport in the cross section of such a kiln (Figure 8.16) and examine the classical transient heat transfer problem in the contest of material processing and kiln control that might affect product quality. From the illustration in Figure 8.16 one can write balance equations in the Lagrangian framework and examine the temperature response and the expansion kinetics of an individual shale particle tumbling down the incline based on its velocity and the fluid-particle heat transfer rate. Assuming the particle emerges at the free surface at a specific temperature T_s and density ρ_0. Within the time the particle travels along the chord length, L_c it will soak up heat and when the temperature reaches a certain threshold, called the bloating temperature, it will undergo an expansion. With little mass loss and large expansion, the density will reduce to form a lightweight aggregate. The dependent property for the balance equation is the conversion, that is, $(\rho_0 - \rho)/(\rho_0 - \rho_f)$ which represents the extent of particle density or specific gravity change. This can be related to the Arrhenius equation as

$$\frac{\partial}{\partial t}\left(\frac{\rho_0 - \rho}{\rho_0 - \rho_f}\right) = -A_0 \exp\left(\frac{-E}{\overline{R}T_s}\right) \tag{8.48}$$

where $\rho(x, 0) = \rho_0$ for $-L/2 \le x \le L/2$. Furthermore, it may be assumed that significant gradients exist within the particle due to the large size particles, typically about 2.5–5 cm, and therefore the dimensionless Biot number is large ($hL/k_s \gg 1$). The unidirectional energy balance on the particle (Figure 8.16b) is

$$\frac{\partial}{\partial t}\left(\rho c_p T\right) = \frac{\partial}{\partial x}\left(k_s \frac{\partial T}{\partial x}\right) - \Delta H A_0 \exp\left(\frac{-E}{\overline{R}T}\right)(\rho - \rho_0) \tag{8.49}$$

I.C. (initial condition)

$$T(x, 0) = T_0 \quad \text{for} \quad -x_{L/2} \le x \le x_{L/2} \tag{8.50a}$$

B.C. (boundary condition)

$$k_s \frac{\partial T}{\partial x}(\pm L/2, t) = h(T_{fb} - T_s) + \sigma\varepsilon\left(T_{fb}^4 - T_s^4\right) = Q \tag{8.50b}$$

For symmetry, if the particle centerpoint is chosen for $x = 0$, the B.C. there is

$$\frac{\partial T}{\partial x}(0, t) = 0 \tag{8.50c}$$

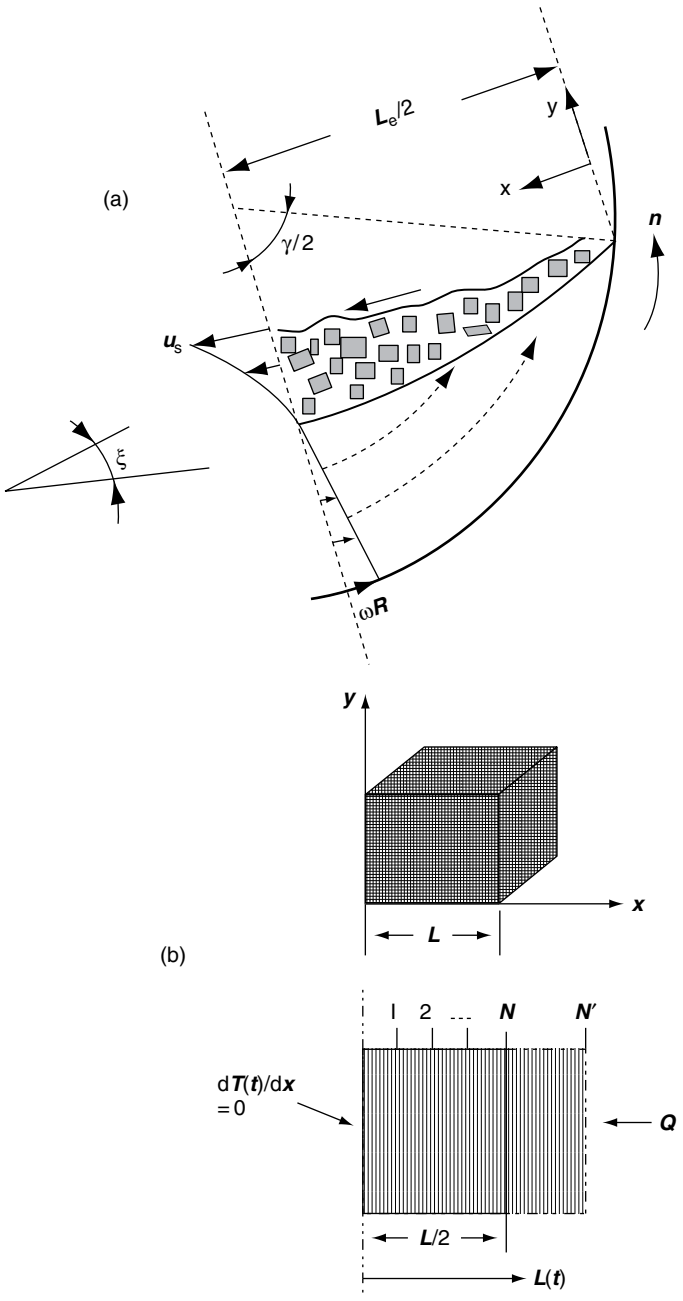

Figure 8.16 Modeling a single particle temperature response using expanded shale kinetics, (a) cross section of kiln, (b) modeled particle (Boateng et al., 1997).

The density or specific gravity change of the shale particle to three-dimensional diffusion will result in a three-dimensional expansion. The incremental change in each direction may be calculated independently using the unidirectional expression

$$\frac{1}{L_0}\frac{\partial L}{\partial t} = \beta_0 \varphi \frac{\partial T}{\partial t} + \beta_f (1-\varphi)\frac{\partial T}{\partial t} + \frac{\eta}{\rho_0}\frac{\partial \rho}{\partial t} \tag{8.51}$$

where L_0 is the initial particle length, L is the instantaneous length, β_0 and β_f are, respectively, the initial and final coefficient of expansion, η is a decomposition or expansion factor and φ is the dimensionless density. The activation energy for dehydroxylation of kaolin in a flash calciner has been reported as ranging between 27 and 70 kJ/mol (Meinhold et al., 1994). The initial density for shale is about 2785 kg/m^3 while the final density, achieved at 1400°C is about 442 kg/m^3 (Boateng et al., 1997).

The system of equations, Equations (8.49) through (8.51), can be solved analytically, graphically, or numerically using implicit finite difference methods utilizing the unidirectional nodal system shown in Figure 8.16b. Since the problem is one-dimensional, it reduces to a system of algebraic equations, $[A][T] = [R']$ where $[A]$ is the coefficient tri-diagonal matrix, $[T]$ is the temperature distribution, and $[R']$ is the set containing residual constant terms. A solution can be found by solving the matrix using the Thomas algorithm with the result shown in Figure 8.17. These results can be plotted using two dimensionless groupings for control of the operation (Figure 8.18). The first grouping is the Peclet number for heat transfer, $Pe(u_s L_c/\alpha)$, and representing the ratio of the heat absorption time to the time of traverse at the exposed bed surface. The second is the modified Damkohler group II grouping, $D\left(\alpha_m/\kappa L_0^2\right)$, where κ is the expansion rate constant in units (1/s), defined as the ratio of the timescales of particle self-diffusion in the active layer and the particle expansion time. This parameter is essentially material dependent and can be related to the activation energy that governs the kinetics of the expansion. Since the surface velocity depends on the rotational rate, Pe is similar to the rotational Froude number $Fr(\omega^2 R/g)$ which is more convenient and practical for an operator.

The graph in Figure 8.18 can be employed as a control procedure for quality assurance. For example, if it is desirable for the lightweight aggregate kiln operator to change the kiln feed rate and maintain the

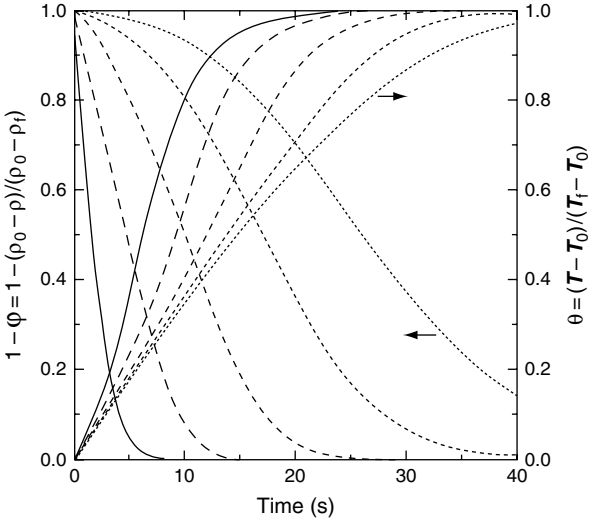

Figure 8.17 Predicted temperature and density changes at the exposure time for shale materials of various origin (Boateng et al., 1997).

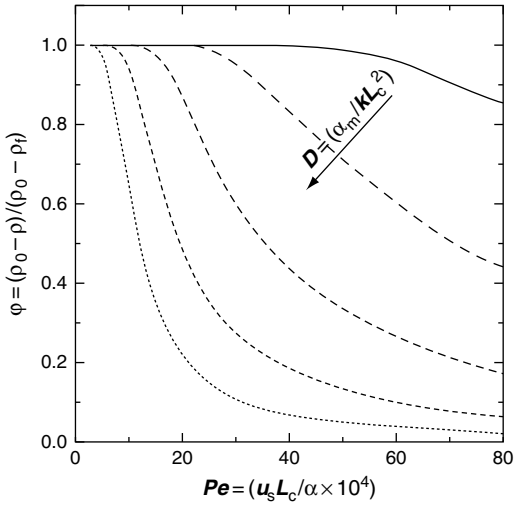

Figure 8.18 Kiln and product quality control curves for shale expansion in a 2.44 diameter rotary kiln (Boateng et al., 1997).

same degree of fill (i.e., constant chord length), then the kiln speed must be altered according to *Pe*. If the heat transfer rate is not changed after this action, then the quality φ will change for that particular material. If each curve represents a specific material, that is, easy to

cook (low E) or hard to cook (high E), then the desired quality can be achieved by following the appropriate path on the curve either by reducing kiln speed or by increasing the heat flux.

References

A. A. Boateng. "On flow-induced kinetic diffusion and rotary kiln bed burden heat transfer," *Chem. Eng. Comm.*, 170, 51–66, 1998.

A. A. Boateng and P. V. Barr. "A thermal model for the rotary kiln including heat transfer within the bed," *Int. J. Heat Mass Transfer*, 39, 2131–2147, 1996.

A. A. Boateng, E. R. Thoen, and F. L. Orthlieb. "Modeling the pyroprocess kinetics of shale expansion in a rotary kiln," *Trans. IChemE*, 75, part A1, 278–283, 1997.

P. V. Barr, J. K. Brimacombe, and A. P. Watkinson. "A heat-transfer model for the rotary kiln: Part I. Pilot kiln trials," *Met. Trans. B*, 20B, 391–402, 1989.

J. K. Brimacombe and A. P. Watkinson. "Heat transfer in a direct fired rotary kiln: Part I. Pilot plant and experimentation," *Met. Trans. B*, 9B, 201–208, 1979.

J. R. Ferron and D. K. Singh. "Rotary kiln transport processes," *AIChE J.*, 37, 774–758, 1991.

J. P. Gorog, T. N. Adams, and J. K. Brimacombe. "Regenerate heat transfer in rotary kilns," *Met. Trans. B*, 13B(2), 153–163, 1982.

J. P. Gorog, T. N. Adams, and J. K. Brimacombe. "Heat transfer from flames in a rotary kiln," *Met. Trans. B*, 14B, 411–424, 1983.

B. G. Jenkins and F. D. Moles. "Modelling of heat transfer from large enclosed flame in a rotary kiln," *Trans. IChemE*, 59, 17–25, 1981.

J. Lehmberg, M. Hehl, and K. Schugerl. "Transverse mixing and heat transfer in horizontal rotary drum reactors," *Powder Technol.*, 18, 149–163, 1977.

R. H. Meinhold, S. Salvador, T. W. Davies, and R. C. T. Slade. "A comparison of the kinetics of flash calcination of kaolinite in different calciners," *Trans. IChemE*, 72(A1), 105–113, 1994.

S. V. Patanker. *Numerical Heat Transfer and Fluid Flow*. Hemisphere, New York, 1980.

A. Sass. "Simulation of the heat transfer phenomenon in a rotary kiln," *I&EC Process Des. & Dev.*, 6(4), 532–535, 1967.

W. Schotte. (1960). "Thermal conductivity of packed beds," *J. AIChE*, 6(1), 63–67, 1960.

W. W. M. Siu and S. H.-K. Lee. "Effective conductivity computation of a packed bed using constriction resistances and contact angle effects," *Int. J. Heat Mass Transfer*, 43, 3917–3924, 2000.

A. J. Slavin, F. A. Londry, and J. Harrison. "A new model for the effective thermal conductivity of packed beds of solid spheroids: Alumina in helium between 100 and 500°C," *Int. J. Heat Mass Transfer*, 43, 2059–2073, 2000.

W. N. Sullivan and R. H. Sabersky. "Heat transfer to flowing granular media," *Int. J. Heat Mass Transfer*, 18, 97–107, 1975.

S. H. Tscheng and A. P. Watkinson. "Convective heat transfer in rotary kilns," *Can. J. Chem. Eng.*, 57, 433–443, 1979.

N. Wakao. "Effect of radiating gas on effective thermal conductivity of packed beds," *Chem. Eng. Sci.*, 28, 1117–1118, 1973.

N. Wakao and D. Vortmeyer. "Pressure dependency of effective thermal conductivity of packed beds," *Chem. Eng. Sci.*, 26, 1753–1765, 1971.

G. W. J. Wes, A. A. H. Drinkenburg, and S. Stemerding. "Heat transfer in a horizontal rotary drum reactor," *Powder Technol.*, 13, 185–192, 1976.